Majorana fermions on the domain wall of marginally twisted bilayer of transition metal dichalcogenides

Richang Huang *
Department of Physics, The University of Hong Kong, Hong Kong, China
and Department of Physics, Southern University of Science and Technology, Shenzhen 518055, China

Dapeng Yu
Shenzhen Institute for Quantum Science and Engineering, and Department of Physics, Southern University of Science and Technology, Shenzhen 518055, China;
International Quantum Academy, Shenzhen 518048, China;
Guangdong Provincial Key Laboratory of Quantum Science and Engineering, Southern University of Science and Technology, Shenzhen 518055, China;
and Shenzhen Key Laboratory of Quantum Science and Engineering, Southern University of Science and Technology, Shenzhen 518055, China

Wang Yao
Department of Physics, The University of Hong Kong, Hong Kong, China
and HKU-UCAS Joint Institute of Theoretical and Computational Physics at Hong Kong, China

(Received 9 June 2023; revised 31 July 2023; accepted 29 August 2023; published 18 September 2023)

We propose to realize two-dimensional superstructures of chiral topological superconductors based on marginally twisted bilayers of transition metal dichalcogenides in proximity to a conventional *s*-wave superconductor. Majorana fermions arise at the domain boundaries of the AB and $A'B'$ stacking domains as a result of a sign flip across the domain wall in a Rashba spin-orbit coupling coefficient at the valence band edge. Unlike previous models that only allow for one Majorana per boundary, each domain wall can host two helical Majorana edge states with the same Majorana polarization, preventing hybridization. This offers a promising alternative platform for studying Majorana physics.

DOI: 10.1103/PhysRevB.108.115307

I. INTRODUCTION

Nowadays a central focus in condensed matter physics is the search for topological states of matter [1–3]. Similar to the well-known quantum Hall state, a chiral topological superconductor with a Bogoliubov–de Gennes (BdG) Chern number $\mathcal{N}$ has a full pairing bulk gap and holds $\mathcal{N}$ topologically protected chiral Majorana fermions on the boundaries [4]. For the $|\mathcal{N}| = 1$ case, the Majorana edge state has only half the degrees of freedom of usual chiral fermions, and a Majorana zero mode in the vortex core [5] would obey non-Abelian statistics [6,7], which makes it potentially valuable for the realization of topological quantum computing [8]. Intensive efforts have been made to search for the chiral topological superconductors in one and two dimensions. Making use of the proximity effect of a conventional *s*-wave superconductor, many different artificial designs to realize topological superconductors have been proposed and experimentally studied during the past years [9–18]. While experimental results have not always been conclusive, the solid theoretical foundations of the field have driven continued progress [19,20].

Due to the interlayer hybridization and the moiré superlattice effects, a layered assembly of two-dimensional materials has provided versatile possibilities to engineer material properties [21]. In marginally twisted bilayer transition metal dichalcogenides (TMDs) of nearly parallel stacking, it has been shown both theoretically [22–24] and experimentally [25–27] that lattice reconstruction can take place and lead to the formation of alternating AB or $A'B'$ stacking domains [Fig. 1(b)], as the energy gain from the expanded areas can overcome the energy cost of domain walls, up to a critical angle $\sim 2.5^\circ$ [28]. With inversion and mirror symmetry breaking, bilayer TMDs of AB and $A'B'$ stacking configurations are known to feature out-of-plane electrical polarization and Rashba spin-orbit coupling at the valence band edge at the Γ point [29]. AB and $A'B'$ domains have opposite signs for both the electrical polarization and Rashba coefficient, as illustrated in Fig. 1(a). This suggests an intriguing possibility to extend the scenario first proposed by Sau *et al.* [11], where a combination of Rashba spin-orbit coupling, magnetic field, and an *s*-wave superconducting gap effectively makes itself a chiral topological *p*-wave superconductor. With alternating signs of the Rashba coefficient between the AB and $A'B'$ domains in marginally twisted bilayer TMDs,, bringing it in proximity to a conventional superconductor and under a magnetic field can lead to superstructures of topological

*huangrc@connect.hku.hk

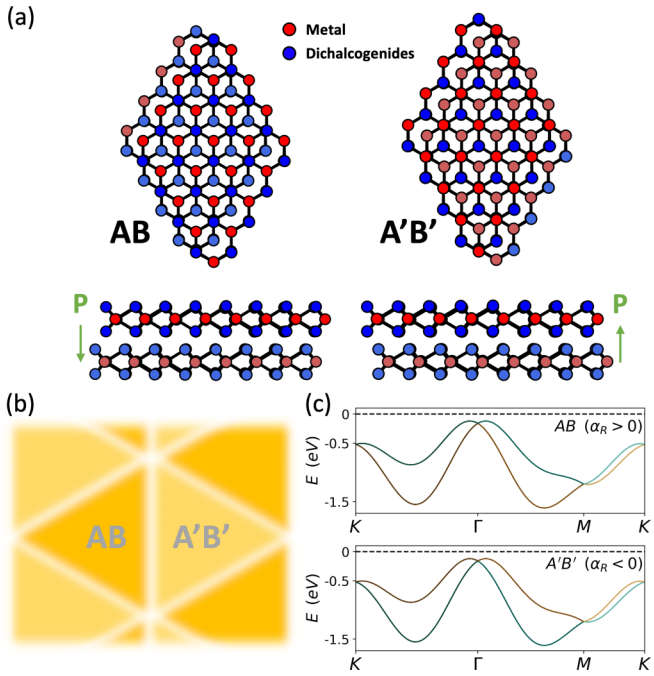

FIG. 1. (a) Top and side views of the AB and $A'B'$ stacking configurations of TMD. P indicates the direction of the out-of-plane electrical polarization arising from inversion and mirror symmetry breaking. (b) Illustration of marginally twisted bilayer transition metal dichalcogenides, where the triangular-shaped domains of $AB/A'B'$ stacking were formed due to lattice reconstruction. (c) Band structures of the AB and $A'B'$ stacking configurations calculated from our tight-binding model with different signs of the Rashba coefficients α_R, where the colors green/brown indicate the sign $+/-$ of the spin σ_y of the eigenstates.

superconductors. We show that this gives the opportunity to engineer Majorana fermions on the domain wall between AB and $A'B'$ stacking domains. Additionally, we have also studied a similar setup but with domain walls between reversed magnetic fields, which could be achieved by placing a ferromagnetic monolayer on an antiferromagnetic substrate [30]. However, as our results show, the chiral edge states in this case are not of the Majorana type.

The organization of this paper is as follows. After this introductory section, Sec. II describes the effective model and parameters we used to simulate the systems. Section III provides a discussion on the mechanism that prevents the two Majoranas on one domain wall from hybridizing. Section IV presents the effects on a moiré superlattice, and Sec. V concludes the paper and gives an outlook.

II. MODEL

The bands in the vicinity of the Fermi energy mainly originate from the d orbitals of the metal atoms. Monolayer TMD has a quasi-two-dimensional (2D) layered structure consisting of stacked units of metal atoms on a triangular lattice sandwiched between chalcogen elements. However, due to the complexity of the structure and the small twisted angle required, a detailed microscopic description of the systems becomes unmanageable. Fortunately the essential features of topological superconductivity are insensitive to the specifics of the model and rely solely on the particle-hole symmetry. Therefore we employ a low-energy phenomenological model to describe the domain wall of a marginally twisted bilayer TMD covered by a conventional superconductor and on a magnetic insulator or subjected to an external magnetic field, in which the Zeeman effect and the superconductivity are introduced. We use a 2D tight-binding Hamiltonian, which corresponds to a discretization of the continuous model [11] on a triangular lattice with primitive vectors $\overrightarrow{a_1} = (a, 0)$, $\overrightarrow{a_2} = (\frac{a}{2}, \frac{\sqrt{3}a}{2})$, and lattice constant $a = 1$,

$$\begin{aligned}\mathcal{H} = &-\sum_{i,j,\sigma} t_{ij} c^\dagger_{i\sigma} c_{j\sigma} - \mu \sum_{i,\sigma} c^\dagger_{i\sigma} c_{i\sigma} \\ &+ i\alpha_R(i) \sum_{\langle i,j\rangle,\sigma,\sigma'} (x_{ij}\sigma_x - y_{ij}\sigma_y)_{\sigma,\sigma'} c^\dagger_{i\sigma} c_{j\sigma'} \\ &+ \sum_{i,\sigma,\sigma'} (V_Z(i)\sigma_z)_{\sigma,\sigma'} c^\dagger_{i\sigma} c_{i\sigma'} \\ &+ \sum_i \Delta(c^\dagger_{i\uparrow} c^\dagger_{i\downarrow} + \text{H.c.}). \end{aligned} \tag{1}$$

Here, $c^\dagger_{i\sigma}$ is the creation operator on site i at location (x_i, y_i) with spin σ. t_{ij} is the hopping amplitudes between site i and site j. μ is the chemical potential. $\alpha_R(i)$ and $V_z(i)$ are the Rashba spin-orbit coupling and the Zeeman splitting given by the magnetic field, which can both be spatially dependent in the discussion below. x_{ij} and y_{ij} are the displacements along each direction when hopping from the nearest neighborhood $\langle i, j\rangle$. Δ is the induced s-wave superconducting pairing. The KWANT package [31] was adopted for parts of the numerical calculations performed. Here, we note that a model similar to Eq. (1) was used in Ref. [32] to successfully describe the topological superconductivity experimentally discovered in the ferromagnet/superconductor heterostructure.

Equation (1) can actually be mapped to two sets of spinless $p \pm ip$-wave superconductors [33]. Consider a ribbon geometry and take $\Delta_e = \frac{\alpha\Delta}{|V_Z|}$, $\mu_e = |V_Z| - \sqrt{\mu^2 + \Delta^2}$. Assuming $\mu_e = -\mu_0$ is a negative constant for $x < 0$ and $\mu_e = +\mu_0$ is a positive constant for $x > 0$, then one can follow the steps for $p \pm ip$-wave superconductors [34] to find the Jackiw-Rebbi solution to the emergence of Majorana edge states for this Hamiltonian near the Γ point,

$$|\psi_{p_y}(x, y)\rangle = e^{ip_y y} \exp\left(-\frac{1}{2|\Delta_e|}\int_0^x \mu_e(x')dx'\right)|\phi_0\rangle, \tag{2}$$

with a constant spinor $|\phi_0\rangle = 1/\sqrt{2}(1 \quad 1)^T$ acting on one set of the effective p-wave basis, and the eigenenergy $E(p_y) = -2|\Delta_e|p_y$ showing a gapless, linear, and chiral dispersion of the Majorana fermion. The chirality is determined by the sign of the BdG Chern number,

$$\mathcal{N} = \frac{1}{2\pi}\iint_{\text{BZ}} \mathbf{\Omega}(\mathbf{k}) \cdot d\mathbf{S}, \tag{3}$$

where $\mathbf{\Omega}(\mathbf{k}) = i[\langle \frac{\partial\psi(\mathbf{k})}{\partial k_x} | \frac{\partial\psi(\mathbf{k})}{\partial k_y}\rangle - \langle \frac{\partial\psi(\mathbf{k})}{\partial k_y} | \frac{\partial\psi(\mathbf{k})}{\partial k_x}\rangle]$ is the Berry curvature.

Though the exact value of each parameter in the model is material dependent, the topological nature does not rely

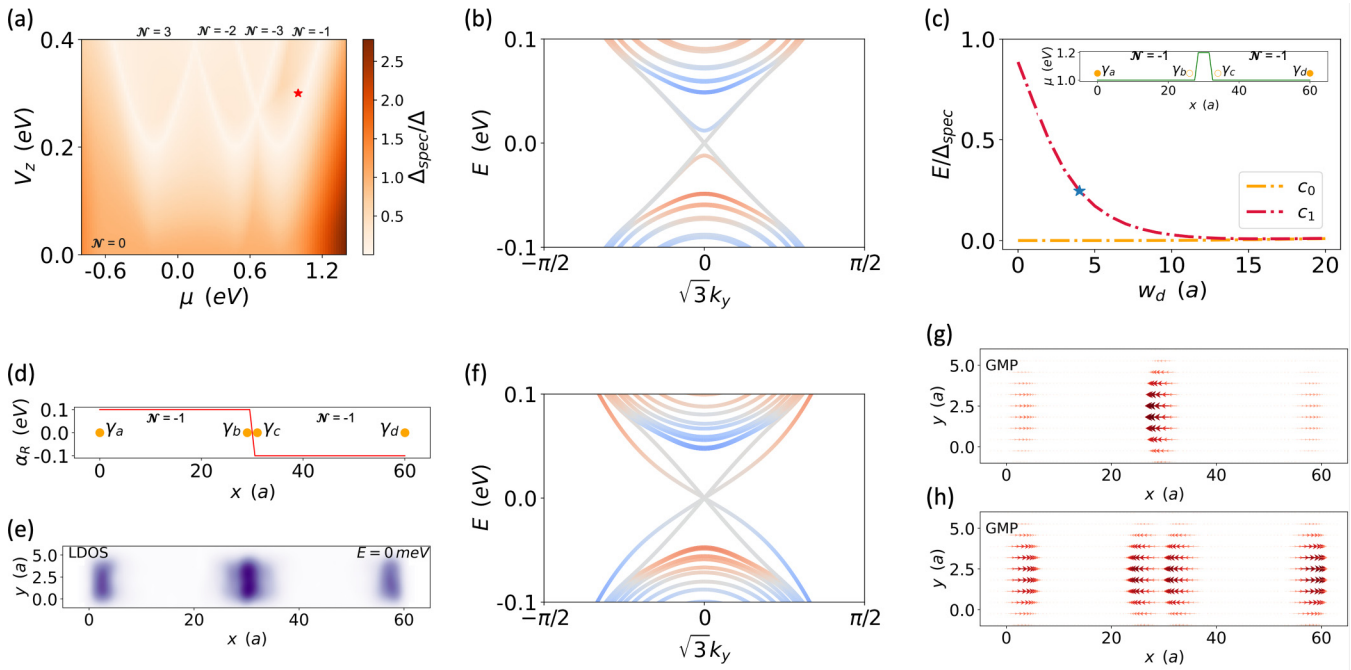

FIG. 2. (a) Phase diagram showing the bulk spectrum gap Δ_{spec} of the model for different sets of (μ, V_z) and the associated BdG Chern number $\mathcal{N}$ for each region. The red star indicates the parameters adopted for the rest of the discussion. (b) Spectrum of the ribbon with a Majorana on the boundaries and a fused fermion on the domain wall. The colors represent particlelike (blue), holelike (red), or charge neutral (gray) bands. (c) Energy of the eigenstates during the process of fusion. The inset shows the profile of the chemical potential domain wall. The solid orange circles represent well-established Majoranas while the open circles represent fused fermions. (d) Profile of the Rashba domain wall. (e) Zero-energy local density of states of the inverse Rashba ribbon. (f) Spectrum of the ribbon with a domain wall of an inverse Rashba coefficient. (g), (h) General Majorana polarization of the two lowest-energy states in the inverse Rashba ribbon.

on the fine-tuned numbers. As shown in Fig. 1(c), we plot the bulk spectrum of our model with $t_1 = -0.03$, $t_2 = -0.1$, $t_3 = -0.01$, which correspond to nearest-, second-nearest, and third-nearest-neighbor hopping, respectively, and $\mu = 1.0$, $\alpha_R = 0.1$ (all energy scales are in the unit of eV) to mimic the valence band calculated in Ref. [29] of bilayer TMD with Rashba spin-orbit coupling. It should be noted that this tight-binding model is not able to recover the whole bands calculated by using the density functional theory (DFT), but is still sufficient to describe the band near the Γ point.

For the heterostructure, which takes the superconducting gap and the Zeeman splitting into account, we plot the bulk spectrum gap Δ_{spec} in Fig. 2(a) for different V_z and μ, normalized by $\Delta = 0.2$ and labeled $\mathcal{N}$ of each region which is calculated efficiently by the numerical method [35]. Here, we note that this exaggerated value of Δ employed here is to reduce the computational complexity (see Appendix A for details). The gap closes, associated with a change of $\mathcal{N}$, indicating a topological phase transition. Unlike most of the previous models, here the vanishing of Rashba spin-orbit coupling at the M and K points leads to an additional gap closing, so that $|\mathcal{N}|$ can take values greater than 1. Detailed discussions about it and the experimental realization of the $|\mathcal{N}| = 3$ case can be found in Ref. [32]. Here, we mainly focused on the effects of spatial varying and the inversion of Rashba α_R on the Majorana edge states. We adopt $V_z = 0.3$ [corresponding to the red star in Fig. 2(a)] for the rest of the discussion so that the Majorana fermions can emerge due to the band inversion at the Γ point.

III. MAJORANAS ON THE DOMAIN WALL

In this section, we investigate the influence of the inversion of Rashba spin-orbit coupling between AB and $A'B'$ stacking domains in marginally twisted TMD by introducing spatially dependent parameters. Recall that the Majorana bound states always come in pairs and two Majorana modes can fuse to a fermionic mode when bringing them close. This process is illustrated in Fig. 2(c) where we manually insert a chemical potential domain wall (corresponding to the $\mathcal{N} = 0$ region) in the center of a topological ribbon geometry with a translational invariant along the y direction and a finite length $L = 60$ along the x direction. As the width of the domain wall w_d decreases, the energy (when $k_y = 0$) of the Majorana pair at the outer sides $c_0 = \frac{1}{\sqrt{2}}(\gamma_a + i\gamma_d)$ remains zero while the energy of the Majorana pair located at the domain wall $c_1 = \frac{1}{\sqrt{2}}(\gamma_b + i\gamma_c)$ increases and eventually merges into the bulk. Figure 2(b) shows a typical spectrum corresponding to the blue star in Fig. 2(c), where the colors represent particlelike (blue), holelike (red), or charge-neutral (gray) bands. The hybridized fermionic mode and its particle-hole partner with a small energy are also referred to as quasi-Majoranas [19].

When the lattice reconstruction take place in the marginally twisted TMD, the moiré supercell is filled by the favored AB and $A'B'$ stacking domains with extremely thin domain walls. For simplicity here we use a step function $\alpha_R(x) = 0.1$ $(x < L/2)$, $-0.1(x \geqslant L/2)$ to imitate the domain wall with an opposite Rashba coefficient on each side as shown in Fig. 2(d). The zero-energy local density of states (LDOS) of the

ribbon with periodic boundaries along the y direction and open boundaries along the x direction is calculated using the kernel polynomial method [36]. Figure 2(e) reveals the emergence of zero-energy Majoranas not only on the vertical boundaries but also at the center of the domain wall.

The spectrum of such a ribbon was plotted in Fig. 2(f), where we can find one pair of Majorana modes with a modified dispersion in addition to the original Majorana pair at the boundaries possessing a linear dispersion. It is worth mentioning that, unlike the more commonly observed chiral Majoranas on the boundaries, the Majorana pair on one domain wall is helical in our scenario, due to the chirality remaining unchanged with the sign flip of the Rashba coefficient, which is verified by calculating $\mathcal{N}(\alpha_R = \pm 0.1) = -1$. Helical Majorana modes can also be accomplished in other platforms such as in Ref. [16] but in which fine-tuned parameters were required.

Trying to illustrate the Majorana nature of these states, we adopt the generalized Majorana polarization [37] (GMP) to visualize the local properties of different edge states as they appeared in different scenarios. In the Nambu basis $C_i = (c_{i\uparrow}, c_{i\downarrow}, c^{\dagger}_{i\downarrow}, -c^{\dagger}_{i\uparrow})^T$, we can write down the antiunitary particle-hole operator as $\mathcal{P} = \sigma_y \tau_y \hat{K}$, where we use $\sigma_{l=x,y,z}$ to denote the Pauli matrices in the spin subspace, $\tau_{l=x,y,z}$ in the particle-hole subspace, and $\hat{K}$ is the complex-conjugation operator. A Majorana by definition should satisfy $\mathcal{P}\gamma = \gamma$ up to an arbitrary phase. Then one can project the operator on site i, $\mathcal{P}_i = \mathcal{P}\hat{r}_i$, and calculate

$$\langle \Psi | \mathcal{P}_i | \Psi \rangle = -2 \sum_{\sigma} \sigma u_{i\sigma} v_{i\sigma} \tag{4}$$

to characterize the local distribution of the GMP for an eigenstate $\Psi = (u_\uparrow, u_\downarrow, v_\downarrow, v_\uparrow)^T$. Note that the expectation values of an antiunitary operator are in vectors in the complex plane and not gauge invariant so that they cannot be used to compare between different states as also mentioned in Ref. [37]. Figures 2(g) and 2(h) plotted the general Majorana polarization of the two degenerate zero-energy bound states formed by the four Majoranas, where we can see the GMPs on the domain wall are always along the same direction. In a hybridized fermionic mode, the two Majoranas should always have opposite polarization. This is because we can always regard one of them to serve as the real part and the other to serve as the imaginary part, so in other words, there is a $\pi/2$ phase difference between them. This leads to a π phase difference in the complex plane after we applied $\mathcal{P}$ to the states. The inverse α_R leads to the inversion of Majorana polarization so that even though the two Majoranas on the domain wall are spatially strongly overlapping, they can maintain the Majorana nature.

An intuitive picture of the emergence of a pair of helical Majorana domain walls can also be seen from the point of stacking one-dimensional topological chains to construct a two-dimensional topological system. Similar to the relation between one-dimensional spinless chains and a quantum (anomalous) Hall system [2], the Hamiltonian for a two-dimensional topological superconductor can also be constructed by stacking one-dimensional chains appropriately. When the sign of the Rashba is flipped, one can always expect α_R to effectively be equal to zero at the domain wall.

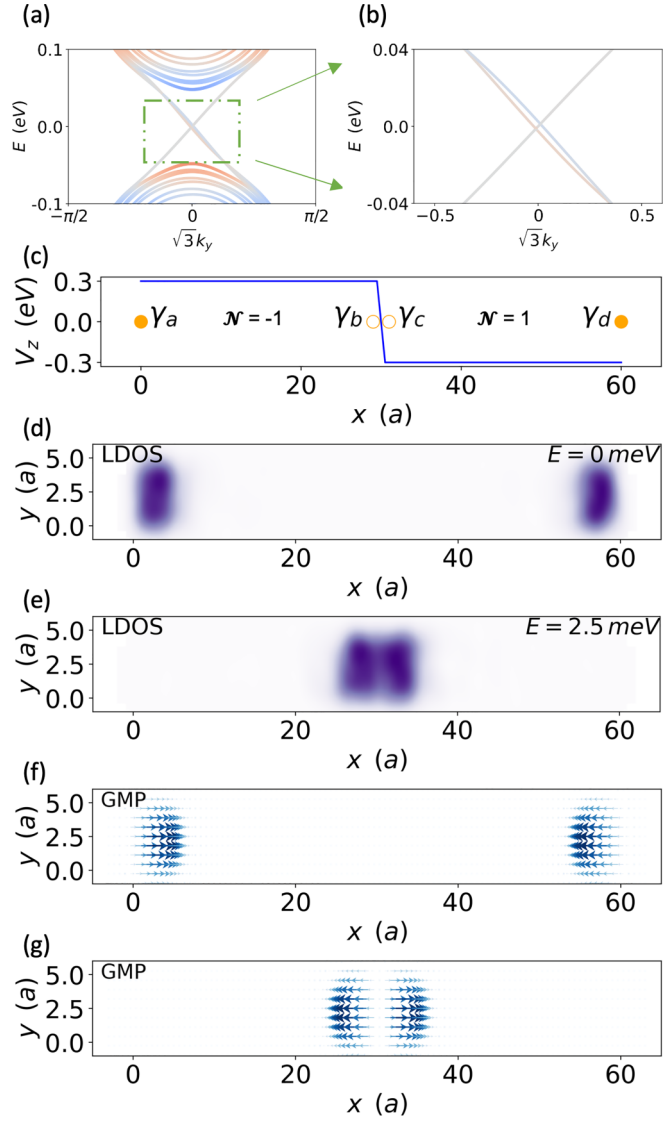

FIG. 3. (a) Spectrum of a ribbon with the domain wall of an inverse Zeeman coefficient. (b) Enlarged center part of (a) where a pair of fermionic modes with negative group velocity can be seen clearly. (c) The profile of a Zeeman domain wall. (d), (e) Local density of states of the inverse Zeeman ribbon at energy $E = 0$ and $E = 2.5$ meV. (f), (g) General Majorana polarization of the two lowest-energy states in the inverse Zeeman ribbon.

Since $\Delta_e = \frac{\alpha\Delta}{|V_Z|}$, the interchain pairing also vanishes, leaving a pair of Majoranas on the wall. We provide a more detailed description and visualization in Appendix B.

In contrast, if we inspect the domain wall with an inverse Zeeman field on each side, the bound states exhibit a different behavior. The dispersion is plotted in Fig. 3(a) with an enlarged center part shown in Fig. 3(b). The BdG Chern number $\mathcal{N}(V_Z = \pm 0.3) = \mp 1$, so that in this case the two Majorana modes on the domain wall would have the same chirality and fuse into a chiral fermion due to the spatial overlapping (the blue and red lines with a negative group velocity), while the other two Majorana edge states remain degenerate as illustrated in Fig. 3(c).

Again we calculated the LDOS of the ribbon. As shown in Figs. 3(d) and 3(e), the zero-energy states are only

distributed on the boundaries, while the small energy fermionic bound state ($E = 2.5$ meV and its particle-hole partner) is concentrated on the center domain wall. We also calculated and plotted the GMP for the lowest and second-lowest states in this case. Aside from the energy, what differs from the previous case is that the direction of the Majorana polarization has flipped across the domain wall as shown in Fig. 3(g). This is consistent with the hybridized fermionic mode we described before.

One may wonder what would happen if we simultaneously invert Rashba and Zeeman fields. Here, we note this because one can always diagonalize the Hamiltonian Eq. (1) into two blocks with spin + and −, where one block is always trivial and the other can be tuned to be topological [38]. In the case of simultaneously inverse Rashba and Zeeman fields, it is just to make the left half of the system spin + topological and the right half of the system spin − topological. Then we would have a Majorana pair appear on the domain wall, but nothing distinctive would occur.

IV. MAJORANAS ON A SUPERLATTICE

Now we investigate the Majorana features on a superlattice in this section. We calculated the dispersion of the one-dimensional superlattice along the x direction with the period L corresponding to the previous sections. This setup of the superlattice formed by domain walls could be accomplished experimentally by a uniaxial tensile strain on one layer of bilayer TMD to adjust the lattice mismatch [39]. In addition, applying an electric field out of plane tends to increase the area of the AB or $A'B'$ stacking regions, which is of intensive current interest in the context of sliding ferroelectricity [40]. This implies opportunities for electrical control on the geometry of the Majorana networks.

In addition, we applied a different profile of $\alpha_R(x)$, artificially constructed, to confirm that the Majorana bound states are coming from the inversion of the sign of Rashba.

As one can see in Figs. 4(a) and 4(b), where we set a homogeneous Rashba $\alpha_R(x) = 0.1$ and a noninverse step Rashba $\alpha_R(x) = 0.1(x < L/2), 0.3(x \geqslant L/2)$, no Majoranas are present in the gap of the mini-Brillouin zone. This helps to confirm that the inversion of the Rashba coefficient is the key to harvesting Majorana fermions in our model.

For different varying behaviors, as shown in Figs. 4(c) and 4(d), we set a linearly varying Rashba $\alpha_R(x) = -0.4x/L + 0.1(x < L/2), 0.4(x - L)/L + 0.1(x \geqslant L/2)$ and a sinusoidal Rashba $\alpha_R(x) = 0.1\sin(2\pi x/L)$. In these cases, every supercell consists of two domain walls (from positive α_R to negative and vice versa) so that two pairs of Majoranas would emerge, and as expected we can see four degenerate Majorana bound states in these two cases (we have checked the fourfold degeneracy of the zero-energy states from the numerical data). The Majoranas are dispersionless in this case since they are bounded to the domain wall of the Rashba. Comparing the results of these subplots of Fig. 4, we can safely say that the details of the profile of $\alpha_R(x)$ have a very limited impact on the topological nature of the emergency of Majoranas.

In Fig. 4(e) we plot the zero-energy local density of states for a (extended) moiré supercell to simulate the marginally twisted TMD. Similar to the ribbon in the previous section,

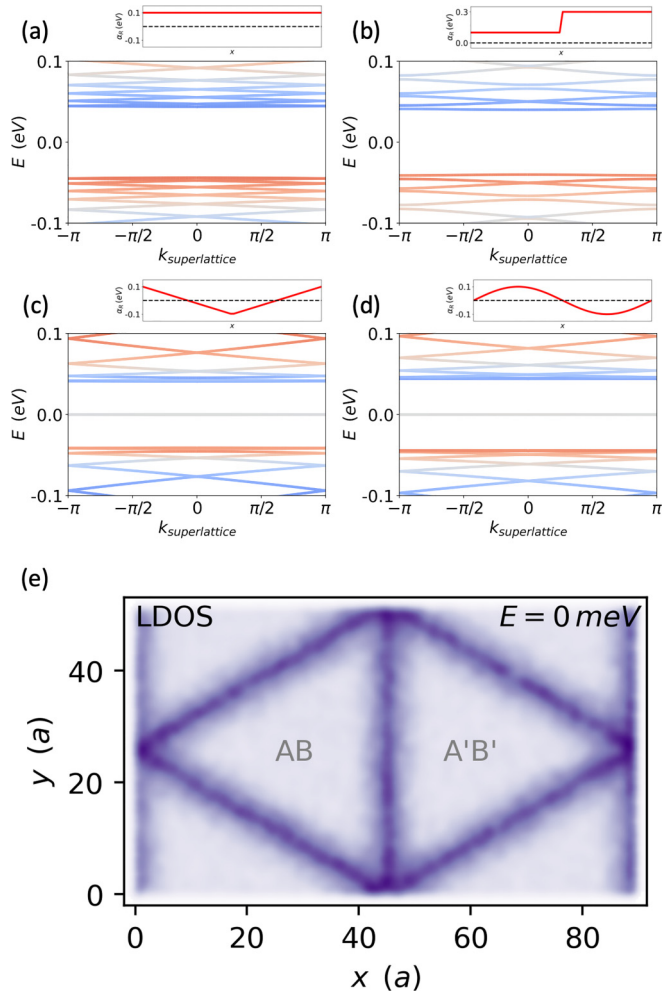

FIG. 4. Superlattice dispersion along the x direction with (a) homogeneous, (b) noninverse step, (c) linearly varying Rashba, and (d) sinusoidal Rashba coefficients. (e) The local density of states of a moiré supercell at zero energy.

the Majoranas concentrate on every domain wall around the triangular AB or $A'B'$ stacking domain as the Rashba coefficient changes its sign across the regions. At the crossing points where three identical domain walls intersect, since the domain walls possess C_3 rotation symmetry, the GMPs residing on the domain wall (not always perpendicular to the wall) are also related to each other by C_3 rotation, so that they cancel each other at the crossing points, and we expect no corner states here. We note that if one could introduce a mass term with different signs for the domain walls crossing at one point, the Majorana edge states would be gapped out and Majorana zero modes could survive in the corner [41]. When the triangle size is finite, similar to previous studies on topological states, hybridization would appear. As long as the system size is much larger than the localization length ($\sim\frac{1}{|\Delta_e|}$) the energy resulting from hybridization is exponentially small [42].

V. CONCLUSION AND DISCUSSION

Spatially varying and inverse Rashba spin-orbit coupling features in marginally twisted TMDs. In this paper, we extended the well-established model and suggested an

alternative platform on the hybrid system. We have shown that in the case of inverse Rashba, the domain wall can host one pair of helical Majorana fermions when the bulk of the system is in the topological phase. On the contrary, in the case of a domain wall with inverse Zeeman or simply a thin topological trivial wall, the associated bound states are fused into fermions.

We also pointed out that inversion of the Rashba spin-orbit coupling results in the Majorana polarization being the same on both sides, preventing their hybridization. There is a similar analogy in one-dimensional nanowires [43], where the so-called Majorana character can save multiple Majorana zero modes at the ends of the wires. However, it should be noted that the Majorana polarization is not solely determined by the Rashba spin-orbit coupling but is also affected by other parameters such as the phase of the superconducting pairing gap and even the Zeeman field, with a complex behavior.

For a realistic system containing a large number of moiré supercells as shown before, the Majorana modes at the boundaries would couple to form a network. The shapes of stacking domains, and meanwhile the shapes of the network, are not always triangular and can be modified by external factors such as strain or electric fields. In other systems such as topological insulators and magnetic topological insulators [39,44], the interplay between topological edge states and moiré effects have been carefully studied. Besides edge states, the interplay of the vortices in this scenario may also show a different phenomenon. There is still unfinished work to be done to unveil the manifestation of Majoranas in this context.

ACKNOWLEDGMENTS

This work was supported by the National Key R&D Program of China (Grant No. 2020YFA0309600), the UGC/RGC of Hong Kong SAR (Grant No. AoE/P-701/20, No. HKU SRFS2122-7S05), the Shenzhen–Hong Kong cooperation zone for technology and innovation (Contract No. HZQB-KCZYB-2020050), and the Innovation Program for Quantum Science and Technology (Grant No. ZD0301703).

APPENDIX A: EFFECT OF Δ SCALING

In the realm of experimental observations, a conventional superconducting pairing gap typically exhibits a magnitude of a few meV, significantly smaller in comparison to other pertinent parameters in our model. In order to achieve an energy resolution capable of discerning details within a few percent of the pairing gap, the computational lattice must possess a linear dimension on the order of thousands of sites, which makes the diagonalization process computationally intensive. To address this issue, it is common practice to employ exaggerated values of the pairing gap and assess the reliability of this approach by examining the scaling behavior of the results [32]. Notably, we have verified through calculations performed on larger scales that our findings obtained using exaggerated values indeed faithfully represent the outcomes that would be obtained with a realistic, smaller value of the pairing gap. This seemingly counterintuitive observation aligns with similar findings in one-dimensional systems, where the localization length remains unaffected by variations in the superconducting gap [45].

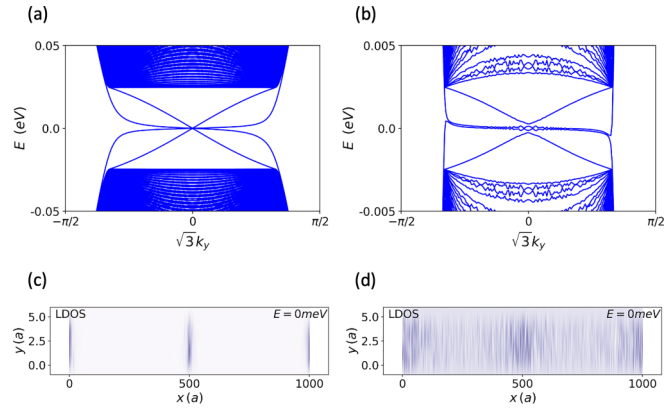

FIG. 5. Spectrum of an $L = 1000$ ribbon with a domain wall of an inverse Rashba coefficient and zero-energy local density of states, where $\Delta = 0.05$ in (a), (c) and $\Delta = 0.005$ in (b), (d). All the other parameters are the same as Fig. 2(f).

As demonstrated in Fig. 5, we present the results of scaling down the pairing gap Δ and calculating the spectrum and LDOS for an inverse Rashba ribbon with a linear dimension of $L = 1000$, considering both $\Delta = 0.05$ and $\Delta = 0.005$. These outcomes generally support previous conclusions; however, noticeable irregular oscillations and blurring are observed in the latter case. Employing smaller values of Δ necessitates larger systems and higher numerical accuracy, which in turn requires increased computational resources. Consequently, in the main body of this paper, an exaggerated value of Δ is adopted.

APPENDIX B: ILLUSTRATION OF THE STACKING PICTURE

As we mentioned in Sec. III, similar to the case of a quantum (anomalous) Hall system [2], the two-dimensional topological superconductor can be constructed from a stacking of one-dimensional spinless chains but with a different interpretation. In the context of a superconductor, the one-dimensional spinless chain is the famous Kitaev chain [46]. When the Kitaev chain is at the topological transition point, it possesses a pair of gapless left- and right-moving modes. One can always stack a bunch of chains to make a two-dimensional system. By

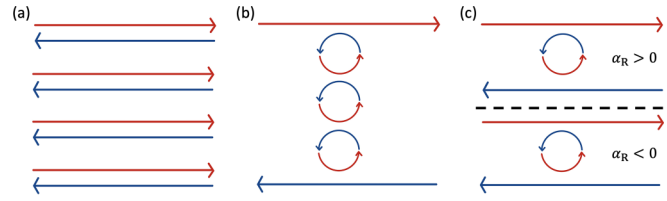

FIG. 6. (a) Direct stacking of one-dimensional chains at the topological transition point into a two-dimensional system. (b) The two-dimensional system can be topological, by setting the interchain coupling appropriately. (c) The interchain coupling vanishes at the Rashba domain wall so that a pair of uncoupled Majoranas are left on the domain wall.

appropriately choosing the interchain coupling terms, one can pair them up into the bulk and leave only one mode at each edge. These edge states are protected by the bulk gap and the spatial separation. By doing this, we would obtain a Hamiltonian topologically equivalent to the two-dimensional topological superconductor. This process is illustrated in Figs. 6(a) and 6(b).

Note that the effective pairing term in the model of this paper $\Delta_e = \frac{\alpha\Delta}{|V_Z|}$ is proportional to the Rashba coefficient. At the domain wall with flipped α_R, one can always find a place at the domain wall with $\alpha_R = 0$ regardless of the detailed profile of the varying α_R, which leads to the interchain coupling vanishing there, so that we can find a pair of helical Majoranas at the domain wall as shown in Fig. 6(c).

[1] M. Z. Hasan and C. L. Kane, Rev. Mod. Phys. **82**, 3045 (2010).
[2] X.-L. Qi and S.-C. Zhang, Rev. Mod. Phys. **83**, 1057 (2011).
[3] M. Sato and Y. Ando, Rep. Prog. Phys. **80**, 076501 (2017).
[4] F. Wilczek, Nat. Phys. **5**, 614 (2009).
[5] G. Volovik, J. Exp. Theor. Phys. Lett. **70**, 609 (1999).
[6] N. Read and D. Green, Phys. Rev. B **61**, 10267 (2000).
[7] D. A. Ivanov, Phys. Rev. Lett. **86**, 268 (2001).
[8] C. Nayak, S. H. Simon, A. Stern, M. Freedman, and S. D. Sarma, Rev. Mod. Phys. **80**, 1083 (2008).
[9] R. M. Lutchyn, J. D. Sau, and S. D. Sarma, Phys. Rev. Lett. **105**, 077001 (2010).
[10] Y. Oreg, G. Refael, and F. v. Oppen, Phys. Rev. Lett. **105**, 177002 (2010).
[11] J. D. Sau, R. M. Lutchyn, S. Tewari, and S. D. Sarma, Phys. Rev. Lett. **104**, 040502 (2010).
[12] X.-L. Qi, T. L. Hughes, and S.-C. Zhang, Phys. Rev. B **82**, 184516 (2010).
[13] V. Mourik, K. Zuo, S. M. Frolov, S. Plissard, E. P. Bakkers, and L. P. Kouwenhoven, Science **336**, 1003 (2012).
[14] S. Nadj-Perge, I. K. Drozdov, J. Li, H. Chen, S. Jeon, J. Seo, A. H. MacDonald, B. A. Bernevig, and A. Yazdani, Science **346**, 602 (2014).
[15] J.-P. Xu, M.-X. Wang, Z. L. Liu, J.-F. Ge, X. Yang, C. Liu, Z. A. Xu, D. Guan, C. L. Gao, D. Qian *et al.*, Phys. Rev. Lett. **114**, 017001 (2015).
[16] J. Wang, Q. Zhou, B. Lian, and S.-C. Zhang, Phys. Rev. B **92**, 064520 (2015).
[17] H.-H. Sun, K.-W. Zhang, L.-H. Hu, C. Li, G.-Y. Wang, H.-Y. Ma, Z.-A. Xu, C.-L. Gao, D.-D. Guan, Y.-Y. Li *et al.*, Phys. Rev. Lett. **116**, 257003 (2016).
[18] S. Manna, P. Wei, Y. Xie, K. T. Law, P. A. Lee, and J. S. Moodera, Proc. Natl. Acad. Sci. USA **117**, 8775 (2020).
[19] H. Pan and S. D. Sarma, Phys. Rev. Res. **2**, 013377 (2020).
[20] D. I. Pikulin, B. v. Heck, T. Karzig, E. A. Martinez, B. Nijholt, T. Laeven, G. W. Winkler, J. D. Watson, S. Heedt, M. Temurhan *et al.*, arXiv:2103.12217.
[21] K. S. Novoselov, A. Mishchenko, A. Carvalho, and A. H. Castro Neto, Science **353**, aac9439 (2016).
[22] M. H. Naik and M. Jain, Phys. Rev. Lett. **121**, 266401 (2018).
[23] S. Carr, D. Massatt, S. B. Torrisi, P. Cazeaux, M. Luskin, and E. Kaxiras, Phys. Rev. B **98**, 224102 (2018).
[24] M. H. Naik, I. Maity, P. K. Maiti, and M. Jain, J. Phys. Chem. C **123**, 9770 (2019).
[25] A. Weston, Y. Zou, V. Enaldiev, A. Summerfield, N. Clark, V. Zólyomi, A. Graham, C. Yelgel, S. Magorrian, M. Zhou *et al.*, Nat. Nanotechnol. **15**, 592 (2020).
[26] Z. Zhang, Y. Wang, K. Watanabe, T. Taniguchi, K. Ueno, E. Tutuc, and B. J. LeRoy, Nat. Phys. **16**, 1093 (2020).
[27] A. Weston, E. G. Castanon, V. Enaldiev, F. Ferreira, S. Bhattacharjee, S. Xu, H. Corte-León, Z. Wu, N. Clark, A. Summerfield *et al.*, Nat. Nanotechnol. **17**, 390 (2022).
[28] V. V. Enaldiev, V. Zólyomi, C. Yelgel, S. J. Magorrian, and V. I. Fal'ko, Phys. Rev. Lett. **124**, 206101 (2020).
[29] Z. Lin, C. Si, S. Duan, C. Wang, and W. Duan, Phys. Rev. B **100**, 155408 (2019).
[30] Q. Tong, F. Liu, J. Xiao, and W. Yao, Nano Lett. **18**, 7194 (2018).
[31] C. W. Groth, M. Wimmer, A. R. Akhmerov, and X. Waintal, New J. Phys. **16**, 063065 (2014).
[32] S. Kezilebieke, M. N. Huda, V. Vaňo, M. Aapro, S. C. Ganguli, O. J. Silveira, S. Głodzik, A. S. Foster, T. Ojanen, and P. Liljeroth, Nature (London) **588**, 424 (2020).
[33] J. Alicea, Phys. Rev. B **81**, 125318 (2010).
[34] B. A. Bernevig, *Topological Insulators and Topological Superconductors* (Princeton University Press, Princeton, NJ, 2013).
[35] T. Fukui, Y. Hatsugai, and H. Suzuki, J. Phys. Soc. Jpn. **74**, 1674 (2005).
[36] A. Weiße, G. Wellein, A. Alvermann, and H. Fehske, Rev. Mod. Phys. **78**, 275 (2006).
[37] N. Sedlmayr and C. Bena, Phys. Rev. B **92**, 115115 (2015).
[38] S.-Q. Shen, *Topological Insulators*, Vol. 174 (Springer, Berlin, 2012).
[39] Q. Tong, H. Yu, Q. Zhu, Y. Wang, X. Xu, and W. Yao, Nat. Phys. **13**, 356 (2017).
[40] M. Wu and J. Li, Proc. Natl. Acad. Sci. USA **118**, e2115703118 (2021).
[41] X. Zhu, Phys. Rev. B **97**, 205134 (2018).
[42] P. Marra, J. Appl. Phys. **132**, 231101 (2022).
[43] N. Sedlmayr, M. Guigou, P. Simon, and C. Bena, J. Phys.: Condens. Matter **27**, 455601 (2015).
[44] C. Xiao, J. Tang, P. Zhao, Q. Tong, and W. Yao, Phys. Rev. B **102**, 125409 (2020).
[45] D. Sticlet, B. Nijholt, and A. Akhmerov, Phys. Rev. B **95**, 115421 (2017).
[46] A. Y. Kitaev, Phys. Usp. **44**, 131 (2001).